Phase-shift calibration errors in interferometers with spherical Fizeau cavities

Peter de Groot

Phase-demodulation algorithms in interferometry often depend on a sequence of evenly spaced reference phase shifts. These phase shifts must be accurately calibrated and can be distorted by geometric effects, especially when spherical components with high curvature are tested. Here the resulting measurement errors are quantified through mathematical analysis, and it is shown that modern phase-estimation algorithms can be effective in a spherical Fizeau cavity with a numerical aperture as large as 0.95.

1. Introduction

Phase-shifting interferometry (PSI) is widely recognized as one of the most important quantitative wave-front measurement techniques currently in use. A PSI instrument is generally composed of an optical interferometer, an electronic imaging system, a computer controller, and a method of precisely adjusting the reference phase of the interferometer.[1–3] The instrument stores interferograms for a series of reference phases; it then applies a mathematical algorithm to recover the original wave-front phase by analysis of the intensity as a function of reference phase shift. Because the wave-front phase itself is a linear function of the surface profile, PSI provides a high-resolution measurement of the surface figure.

The measurement uncertainty and the achievable accuracy of PSI are of great interest, and several papers have concentrated on error analysis.[4–7] In addition, most popular articles in trade journals geared toward getting the best-performance PSI include a discussion of common error sources.[8] One recurring concern is the fidelity of the phase shift. A common method of phase shifting relies on mechanical translation of the reference surface. The total required mechanical motion is normally less than the wavelength of light, and it is supplied by a piezoelectric transducer (PZT) or equivalent assembly, which is calibrated to provide accurate and repeatable phase shifts.[9] There are several factors that effect this calibration, resulting in distorted phase shifts and systematic errors in the phase measurement calculation.

Moore and Slaymaker[10] showed that phase-shift calibration is particularly important when one works with spherical Fizeau cavities. Because the reference surface of a spherical cavity is curved, the phase shift caused by axial translation is not uniform over the field of view. In the extreme case in which a reference surface has a N.A. of 1.0, the edge of the interference pattern is not shifted in phase at all. Creath and Hariharan[11] showed that standard methods of phase estimation in PSI are adequate for N.A. < 0.63, and they suggested a modified geometry for higher N.A.'s that uses an auxiliary flat reference with highly corrected spherical optics. Another possibility is wavelength-shift PSI instead of mechanical phase shifting.[12] Because these solutions require a significant investment in hardware, it is worth having a second look at the performance limitations of mechanical PSI with curved reference surfaces.

In this paper I reexamine the problem of phase-shift calibration, with the objective of determining the maximum N.A. for a spherical Fizeau interferometer with an axial phase shift. This study assumes some flexibility in the choice of a PSI algorithm, but it is restricted to methods that involve a sequence of data frames acquired at approximately equal phase intervals. Another restriction is the exclusion of any method that requires knowledge of the cavity configuration, which would complicate the use of the instrument. These restrictions and others that become evident in the presentation are typical of modern commercial interferometers.

As part of this study I derive an exact formula for the phase error by using Fourier analysis and the concept of data-sampling windows. This formula

The author is with Zygo Corporation, Laurel Brook Road, Middlefield, Connecticut 06455.

Received 24 September 1993; revised manuscript received 31 August 1994.

0003-6935/95/162856-08$06.00/0.

permits rapid evaluation of algorithms without numerical simulation. An important conclusion of this study is that modern PSI algorithms have solved the problem of linear phase errors for most applications in interferometry, including spherical cavities with N.A.'s as high as 0.95.

2. Phase Estimation in Phase-Shifting Interferometry

The objective of surface-profiling PSI is to measure the reflected wave-front phase, θ, as a function of the surface coordinates. The phase-estimation procedure in PSI requires a sequence of $N \geq 3$ interference images, each having a different phase offset ϕ_j, where $j = 0 \ldots N - 1$. Each sample is commonly called a frame or a bucket, and the phase shifts are typically introduced by mechanical displacement of the reference surface of the interferometer. For practical reasons and for ease in the data processing, phase shifts ϕ_j are linear in time and are characterized by a phase increment, α_0.

For a given pixel in the field of view, the intensity samples in the two-beam approximation are

$$g_j = Q[1 + V \cos(\theta + \phi_j)], \tag{1}$$

where V is the fringe visibility, Q is a constant, and

$$\phi_j = (j - j_0)\alpha_0. \tag{2}$$

In Eq. (2) j_0 is a constant offset that is not necessarily an integer. Most generally, PSI algorithms for calculating phase θ are of the form

$$\theta = \tan^{-1}\left(\frac{\sum s_j g_j}{\sum c_j g_j}\right) + \text{const}, \tag{3}$$

where s_j and c_j are constant coefficients. For example, a popular algorithm that uses an $\alpha = \pi/2$ phase step is the Schwider–Hariharan or five-bucket algorithm[13,14]:

$$\theta = \tan^{-1}\left[\frac{2(g_1 - g_3)}{2g_2 - (g_0 + g_4)}\right]. \tag{4}$$

The nonzero coefficients in this case are $s_1 = 2$, $s_3 = -2$, $c_0 = -1$, $c_2 = 2$, and $c_4 = -1$. Although there are many other approaches to phase estimation in interferometry, the temporal PSI method described here involving an algorithm of the form shown in Eq. (3) is representative of common practice.

3. Errors in the Phase Increment

The validity of Eq. (3) and hence the correct application of PSI algorithms depend to a great extent on the proper calibration of the phase shift. Suppose that instead of the assumed phase shifts α_0 as in Eq. (2), we have

$$\alpha = (1 - \varepsilon)\alpha_0, \tag{5}$$

where α is the actual phase increment and ε is the calibration error. The phase shifts are now

$$\phi_j' = (\alpha/\alpha_0)\phi_j. \tag{6}$$

Because PSI algorithms are designed for specific phase increments, they cannot be expected to perform perfectly if the increment is incorrect. Calibration error ε is a function of a number of different experimental parameters, some of which cannot be controlled or entirely eliminated by calibration procedures. These parameters include tilting or twisting of the PZT pusher during translation, and geometrical effects that arise when one is working with fast spherical cavities.

Tilt during translation may be thought of as a PZT gain $\gamma(x, y)$ that is a function of the coordinates (x, y) in the reference plane of the interferometer:

$$\gamma(x, y) = \gamma_0 + x\gamma_x + y\gamma_y. \tag{7}$$

This gain can be normalized so that in an ideal interferometer, the coefficients in Eq. (7) would be $\gamma_0 = 1$, $\gamma_x = 0$, $\gamma_y = 0$. Most commercial systems have automatic calibration procedures to approach this ideal condition as nearly as possible.

The other major source of error in phase modulation is a PZT translation that is not perpendicular to the reference surface. The reciprocal motion of the PZT modulators then translates into a phase modulation that is proportional to the cosine of angle φ between the normal to the reference surface and the direction of motion. One way this can happen is if the PZT pusher is misaligned with respect to the optical axis of the interference cavity, so that there is a sideways motion of the reference surface with respect to the optical axis of the cavity during translation. Another unavoidable source of geometric error occurs with curved reference surfaces as a consequence of the variable inclination of the surface with respect to the direction of PZT travel.

Geometric contributions to calibration error ε can be calculated by the determination of angle φ between the vectors shown in Fig. 1. Unit vector $\hat{\mathbf{p}}$ is oriented in the direction of the PZT motion, whereas vector $\hat{\mathbf{r}}$ is the normal to the reference surface, which for nulled interference fringes is collinear with a geometric ray trace through the cavity. A property of unit vectors is that the dot product is equal to the cosine of the angle between the vectors. Using this principle and the PZT gain $\gamma(x, y)$ defined by Eq. (7), we can write the following general expression for calibration error ε:

$$\varepsilon = 1 - \gamma(x, y)\hat{\mathbf{p}} \cdot \hat{\mathbf{r}}. \tag{8}$$

Equation (8) now includes all of the first-order mechanical contributions to the calibration error. Note, however, that Eq. (8) does not take into account any second-order effects caused by the change in cavity radius. These second-order effects are important in microscopic cavities[15] because they lead to

nonlinear phase shifting, but they will not be considered here.

It is useful to relate the vector quantities to simple scalar values, such as the radius, R, of the reference sphere and coordinates (x, y). Let us define a rectilinear coordinate system with unit vectors $\hat{\mathbf{n}}_x$, $\hat{\mathbf{n}}_y$, $\hat{\mathbf{n}}_z$ such that the z coordinate is along the optical axis of the cavity and the (x, y) coordinates are in a plane perpendicular to the axis. From Figure 1 we can see that the unit ray vector, $\hat{\mathbf{r}}$, normal to the curved reference surface is

$$\hat{\mathbf{r}} = -\frac{x}{R}\hat{\mathbf{n}}_x + -\frac{y}{R}\hat{\mathbf{n}}_y + \frac{R'}{R}\hat{\mathbf{n}}_z, \tag{9}$$

where

$$R' = [R^2 - (x^2 + y^2)]^{1/2}, \tag{10}$$

and R is the radius of curvature of the reference sphere. If the PZT motion is not perfectly aligned with the optical axis of the cavity, then two directional cosines, ξ_x, ξ_y, can be used to describe its orientation with respect to our coordinate system:

$$\hat{\mathbf{p}} = \xi_x\hat{\mathbf{n}}_x + \xi_y\hat{\mathbf{n}}_y + \rho\hat{\mathbf{n}}_z, \tag{11}$$

where

$$\rho = [1 - (\xi_x^2 + \xi_y^2)]^{1/2}. \tag{12}$$

Inserting these expressions into Eq. (8) yields

$$\varepsilon = 1 - (\gamma_0 + x\gamma_x + y\gamma_y)\frac{R'\rho - x\xi_x - y\xi_y}{R}. \tag{13}$$

This is the complete equation for calibration errors caused by tilt, focus, and alignment effects in a spherical cavity.

In many practical situations involving fast spherical cavities, gain $\gamma(x, y)$ is carefully controlled, and the greatest source of error is the variation in quantity R'. This error is fundamental to the geometry of a Fizeau cavity having a spherical reference surface and cannot be completely eliminated without fundamental changes in the phase-shift mechanism. However, one can improve the situation somewhat by adjusting gain γ_0 to reduce the maximum calibration error across the surface. One approach suggested by Moore and Slaymaker is to make the error at the origin $x = 0, y = 0$ equal in magnitude to the maximum error at the edge of the field of view.[10] This condition is satisfied in the present formalism when

$$\gamma_0 = \frac{2}{2 - \varepsilon_1}, \tag{14}$$

where ε_1 is the maximum error for $\gamma_0 = 1$.

Three error curves for a perfectly aligned spherical cavity are shown in Fig. 2. These curves are generated from Eqs. (13) and (14) as a function of normalized coordinate x/X, where X is the largest x value. The y coordinate is set to zero. The three curves correspond to three different N.A.'s defined by

$$\text{N.A.} = X/R. \tag{15}$$

As a way to get a better idea of the relationship between N.A. and calibration error, it is useful to rearrange the equations to solve for the N.A. as a function of the maximum allowable calibration error. From Eqs. (13), (14), and (15), the result for a perfectly aligned cavity is

$$\text{N.A.}(\varepsilon_{\max}) = \left(1 - \frac{1 - \varepsilon_{\max}}{1 + \varepsilon_{\max}}\right)^{1/2}. \tag{16}$$

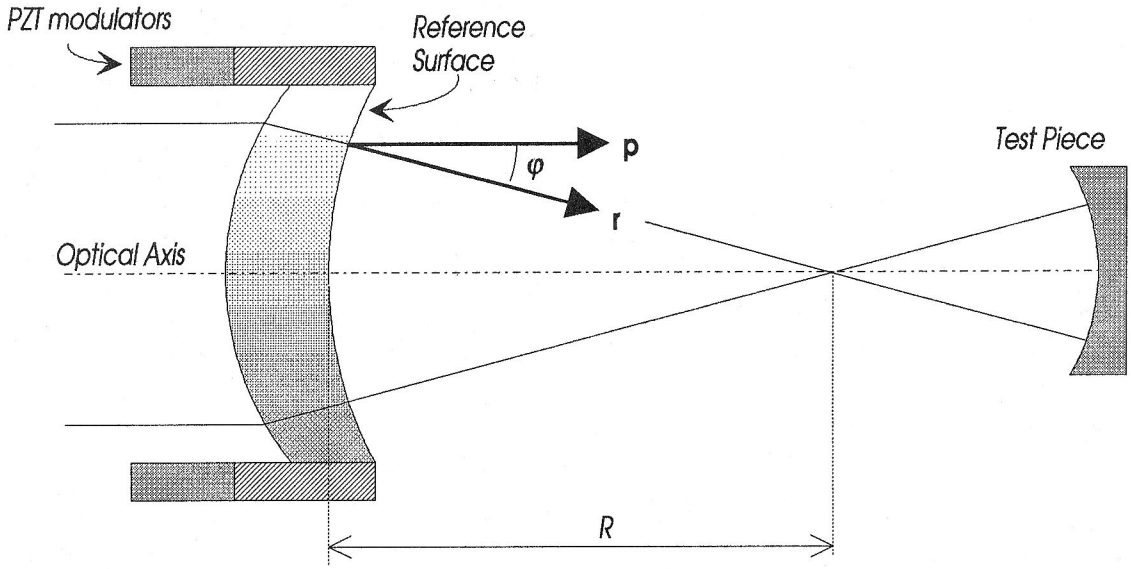

Fig. 1. Spherical Fizeau interferometer cavity. The PZT assembly translates the reference surface axially, thereby shifting the mean phase of the interference pattern. The amount of shift varies with angle φ between radius vector $\hat{\mathbf{r}}$ and translation vector $\hat{\mathbf{p}}$.

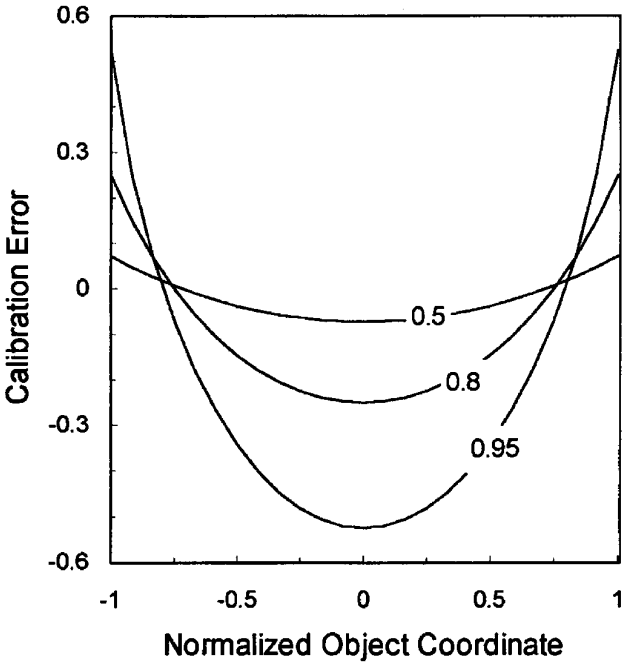

Fig. 2. Phase-shift error ε as a function of normalized field coordinate x/X in a spherical Fizeau interferometer cavity.

Equation (16) is plotted in Fig. 3. If the maximum allowable calibration error, ε_{max}, for a given algorithm is known, then the corresponding maximum N.A. can be determined from the figure or directly from Eq. (16).

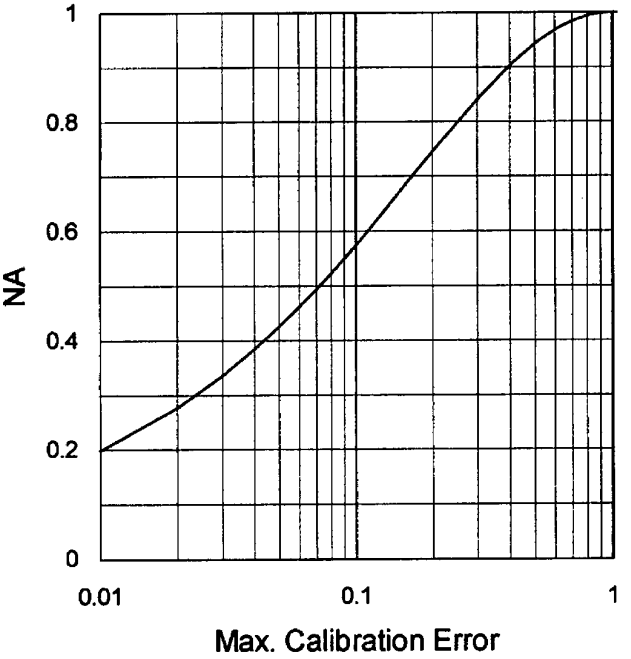

Fig. 3. Maximum N.A. for a spherical Fizeau cavity as a function of maximum allowable calibration error ε_{max}. The maximum calibration error is characteristic of the PSI algorithm.

4. Phase-Shifting Interferometry Measurement Errors

Because a certain amount of calibration error appears to be unavoidable with spherical Fizeau cavities, it is important to quantify the resulting phase measurement errors in order to define a maximum allowable calibration error, ε_{max}. There are three common ways in which this problem is approached in the literature: numerical simulation, linear approximation, and case-by-case mathematical analysis. I first discuss these traditional approaches before presenting an alternative formalism based on the concept of data-sampling windows.

The various papers by Creath and co-workers represent the numerical simulation method of error analysis.[16–18] Some of these simulations are performed by the variation of a known phase θ over a 2π range in as many as 1000 individual steps. A computer calculates the corresponding intensities g_j, processes them through the PSI algorithm, and determines the phase-estimation error, $\Delta\theta$, as a function of the known phase, θ. The computer repeats this procedure over a range of calibration errors and plots the results. A numerical simulation has the advantage of being completely flexible, because many kinds of errors can be quantified by essentially the same computer program. On the one hand, the method can be criticized for being somewhat tedious and for not providing any physical insight into the source of the observed errors. On the other hand, a more sophisticated mathematical analysis will generally be checked against a numerical simulation to verify its validity.

Much of the time calibration errors ε and corresponding phase-estimation errors $\Delta\theta$ are small, so it is possible to gain some insight through approximation.[19] Propagating the error through Eq. (3) for small ε leads to an approximate analytical expression. Schwider and co-workers[13,20] and others have shown that the lowest-order θ-dependent error team varies sinusoidally at twice the rate of the interference fringes themselves, leading to a systematic error or ripple in surface maps. To lowest order in ε, the peak-to-valley (P–V) error, E, of the ripple for the five-bucket algorithm is

$$E \approx \frac{(\pi\varepsilon)^2}{8}. \tag{17}$$

Because the error has a second-order dependence on ε, the five-bucket algorithm is considered highly robust. However, linear approximations such as this one are not adequate for the large calibration errors encountered in spherical Fizeau cavities, although it does give an indication of which algorithms will probably have the best performance.

A third approach to the calculation of phase errors is to insert the error into the PSI algorithm and try and simplify the result as much as possible without making an approximation. In many cases this results in a useful formula. For example, the five-

bucket algorithm can be rewritten for a nearly arbitrary phase increment $0 < \alpha < \pi$ as

$$\theta = \tan^{-1}\left[\frac{2(g_1 - g_3)}{2g_2 - (g_0 + g_4)}\sin(\alpha)\right]. \tag{18}$$

Multiple-wavelength interferometers sometimes makes use of formulas of this kind to compensate for known variations in the phase increment.[21] Joenathan also provided several examples of a case-by-case analysis of PSI algorithms as part of an effort to reduce estimation errors.[22]

Although these traditional methods of error analysis have all been useful in the development of PSI, none of them provides a general analytical formula for P-V error over a large range of calibration values. My purpose of Section 5 is to derive such a formula that is valid for all PSI algorithms having the form shown in Eq. (3).

5. General Formula for Calibration Errors

PSI in general and Eq. (3) in particular can be interpreted mathematically as a phase-estimation process that involves a discrete Fourier transform (DFT).[23] The advantage of the DFT formalism is that it is much easier to analyze the effect of various errors in the phase-shifting process in a general way. From the DFT point of view, the phase angle is calculated from

$$\theta = \arg(G) + \text{const}, \tag{19}$$

where G is the DFT of intensity g_j in Eq. (1):

$$G = \sum_j g_j w_j \exp(-i\phi_j). \tag{20}$$

The weighting values, w_j, correspond to a data-sampling window. Although the concept of a data-sampling window is characteristic of Fourier transform methods of frequency and phase estimation, it is unusual in the context of PSI. This is because traditional PSI algorithms for surface metrology typically employ such a small number of data samples that there is not much opportunity to manipulate the sampling window. However, frequency-domain analysis of PSI is an effective means of understanding error sources even with sparse data sampling.[24]

By comparing Eqs. (19) and (20) with Eq. (3), we see that

$$s_j = \text{Im}[w_j \exp(-i\phi_j)], \tag{21}$$

$$c_j = \text{Re}[w_j \exp(-i\phi_j)], \tag{22}$$

and inversely

$$w_j = [s_j \sin(-\phi_j) + c_j \cos(\phi_j)] + i[s_j \cos(\phi_j) - c_j \sin(-\phi_j)]. \tag{23}$$

Thus the five-bucket algorithm is based on a window with coefficients $w_0 = w_4 = 1$ and $w_1 = w_2 = w_3 = 2$. Typically the windows for error-compensating PSI algorithms are approximately bell shaped when represented graphically.

The description of PSI in terms of windows and DFT's provides a useful way of predicting errors when the signal is less than ideal. In fact, Eqs. (19) and (20) are valid only for signals that have exactly the desired phase increment. Suppose a nonideal input signal, g_j', has a phase increment of $\alpha \neq \alpha_0$. The DFT of this signal is

$$G'(\alpha, \theta) = Q \sum_j \left\{1 + V\cos\left[\theta + \left(\frac{\alpha}{\alpha_0}\right)\phi_j\right]\right\} w_j \exp(-i\phi_j), \tag{24}$$

which evaluates to

$$G'(\alpha, \theta) = Q[W(\alpha_0) + \tfrac{1}{2}V[W(\alpha_0 - \alpha)\exp(i\theta) + W(\alpha_0 + \alpha)\exp(-i\theta)]], \tag{25}$$

where

$$W(\alpha) = \sum_j w_j \exp\left(\frac{-i\phi_j\alpha}{\alpha_0}\right) \tag{26}$$

is the DFT of the window function. We see immediately that angle θ is linearly proportional to the argument of $G'(\alpha, \theta)$ only if the terms $W(\alpha_0)$ and $W(\alpha_0 + \alpha)$ are both zero.

Constructing a window such that $W(\alpha_0) = 0$ is no problem, because it is sufficient to have numerator coefficients s_j and denominator coefficients c_j sum to zero. The difficulty is in the term $W(\alpha_0 + \alpha)$, which is due to leakage from the negative-frequency portion of the Fourier spectrum. Assuming that the dc contribution $W(\alpha_0)$ has been eliminated, we can write

$$\theta = \arg[G'(\alpha, \theta)] - \Delta\theta(\alpha, \theta) + \text{const}, \tag{27}$$

where

$$\Delta\theta(\alpha, \theta) = \arg\left[\frac{W(\alpha_0 - \alpha) + W(\alpha_0 + \alpha)\exp(-2i\theta)}{W(0)}\right]. \tag{28}$$

is the error in the phase estimate.

Equation (28) can be rewritten in terms of calibration error ε as follows:

$$\Delta\theta(\varepsilon, \theta) = \arg[W_0(\varepsilon) + W_2(\varepsilon)\exp[-2i\theta + i\zeta(\varepsilon)]] + \xi(\varepsilon), \tag{29}$$

where

$$W_0(\varepsilon) = \left|\frac{W(\varepsilon\alpha_0)}{W(0)}\right|, \tag{30}$$

$$W_2(\varepsilon) = \left|\frac{W[(2 - \varepsilon)\alpha_0]}{W(0)}\right|, \tag{31}$$

$$\xi(\varepsilon) = \arg\left[\frac{W(\varepsilon\alpha_0)}{W(0)}\right], \tag{32}$$

$$\zeta(\varepsilon) = \arg\left\{\frac{W[(2-\varepsilon)\alpha_0]}{W(0)}\right\} - \xi(\varepsilon). \tag{33}$$

Equation (29) is an exact formula for the error in the phase estimate in PSI as a function of calibration error ε and actual phase θ of the interference signal. It is valid for any PSI algorithm that can be put in the form shown in Eq. (3).

In the evaluation of PSI algorithms, the P–V excursion, $E(\varepsilon)$, of phase error $\Delta\theta(\varepsilon, \theta)$ is of special interest. The P–V error can be found by the calculation of the extrema of $\Delta\theta(\varepsilon, \theta)$ with respect to θ. Within the range $-1 < \varepsilon < 1$, these extrema occur when

$$\cos[-2\theta + \zeta(\varepsilon)] = -\frac{W_2(\varepsilon)}{W_0(\varepsilon)}. \tag{34}$$

Inserting this back into the equation for $\Delta\theta(\varepsilon, \theta)$ results in the relatively simple formula

$$E(\varepsilon) = 2\tan^{-1}\left\{\frac{W_2(\varepsilon)}{[W_0(\varepsilon)^2 - W_2(\varepsilon)^2]^{1/2}}\right\}. \tag{35}$$

This is an exact formula for the P–V error, which is also valid for all PSI algorithms that have the form represented by Eq. (3). For many applications the following small-error approximation may be adequate:

$$E(\varepsilon) \approx 2W_2(\varepsilon). \tag{36}$$

The P–V error is proportional to the magnitude of the normalized Fourier transform of the data-sampling window, evaluated at $\alpha = (2-\varepsilon)\alpha_0$. Equation (36) clearly shows the close relationship between PSI performance and the frequency-domain response of the window function.

A largely neglected effect with extreme phase-shift errors is the decline in signal strength. Looking at Eq. (25) and taking advantage of Eq. (30), we find it evident that apparent fringe contrast $V'(\varepsilon)$ is

$$V'(\varepsilon) = V W_0(\varepsilon). \tag{37}$$

The larger the data window the more rapidly the fringe contrast decreases with calibration error.

6. Example Algorithms

Algorithms for PSI having the form shown in Eq. (3) are traditionally classified according to the number of data samples or buckets. This is becoming less satisfactory because the literature now provides a large choice of algorithms of various sizes and shapes, all designed to optimize performance. This is not the place to review these algorithms exhaustively, even within the narrow context of resistance to calibration errors. However, a few examples will help to illustrate the positive effect of an intelligent choice of data-sampling window. Fortunately these examples are all of different lengths and so will be referred to compactly by the number of data samples. All of the following examples are based on an $\alpha_0 = \pi/2$ phase increment.

Until a few years ago, the most common algorithm in surface-profiling PSI used only four buckets:

$$\theta = \tan^{-1}\left(\frac{g_0 - g_2}{g_1 - g_3}\right). \tag{38}$$

This algorithm has the simplest window, because $w_j = 1$ for $j = 0 \ldots 3$. A square window transforms to a sinc function in the frequency domain, which is characterized by oscillations or sidelobes that continue far from the fundamental frequency of the interferometer. Consequently the four-bucket algorithm is sensitive to negative-frequency leakage and does not perform well in the presence of calibration errors. However, this algorithm is computationally efficient and can be executed at high speed.

From the point of view of data windows, one can improve the situation by summing two mutually offset windows together in such a way as to suppress the sidelobes in the frequency domain. This implicitly is the averaging method proposed by Schwider and co-workers.[13,25] Alternatively, algorithms can be constructed by integer approximation to well-known analytical windows used in digital signal processing.[26] Both methods lead to the five-bucket algorithm introduced above as Eq. (5). Either procedure can also be used to derive the following seven-bucket algorithm[27]:

$$\theta = \tan^{-1}\left[\frac{(g_0 - g_6) - 7(g_2 - g_4)}{4(g_1 + g_5) - 8g_3}\right]. \tag{39}$$

The seven-bucket algorithm has window coefficients $w_0 = w_6 = 1$, $w_1 = w_5 = 4$, $w_2 = w_4 = 7$, and $w_3 = 8$, and it closely approximates a raised-cosine or Von Hann window.[28] The five- and seven-bucket algorithms have improved resistance to calibration errors when compared with the four-bucket algorithm, while at the same time preserving the computational efficiency of integer math.

As a final example, I present here an algorithm that uses floating-point computations and that has extremely high resistance to calibration error. The algorithm is something of a limiting case rather than a practical example, and it is included to show just how good a phase estimate can be when the PSI algorithm closely follows a high-performance data-sampling window. The algorithm is derived from the four-term Blackman–Harris window[29] and requires 15 data samples:

$$\theta = \tan^{-1}\left[\frac{-0.006(g_0 - g_{14}) + 0.166(g_2 - g_{12}) - 0.87(g_4 - g_{10}) + 1.828(g_6 - g_8)}{-0.043(g_1 + g_{13}) + 0.435(g_3 + g_{11}) - 1.392(g_5 + g_9) + 2g_7}\right]. \tag{40}$$

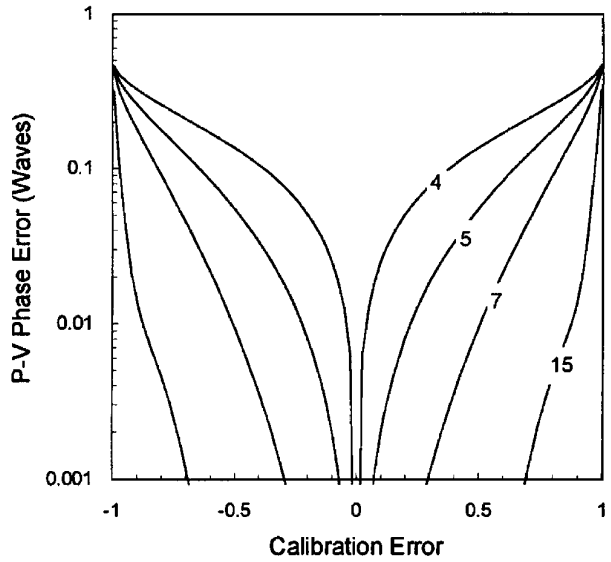

Fig. 4. P–V excursion of periodic phase errors as a function of calibration error ε for four different PSI algorithms. All of these example algorithms have a nominal $a_0 = \pi/2$ phase shift. Actual phase shift α is equal to $(1 - \varepsilon)\alpha_0$.

The window for this algorithm has better than −90-dB sidelobe suppression in the frequency domain.

The P-V phase-estimation errors, $E/2\pi$, as a function of calibration error ε for the four algorithms are plotted together in Fig. 4. The errors were calculated from the exact formula (35) and are valid over the entire $0 < \alpha < \pi$ range. The curves in Fig. 4 show that the choice of algorithm is very important when dealing with the large calibration errors that are typical of fast spherical Fizeau cavities. Figure 5 shows corresponding relative fringe contrast $V'(\varepsilon)/V$ for these algorithms. Generally all of the examples provide a sufficient signal-to-noise ratio for errors as large as $\varepsilon = \pm 0.5$, but only the seven-bucket and

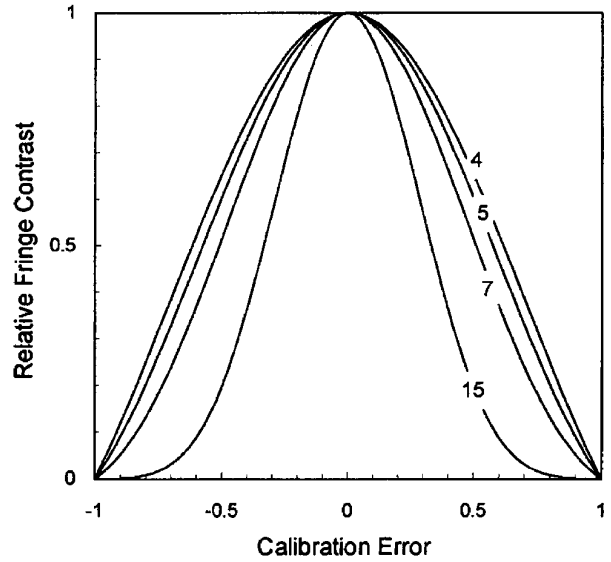

Fig. 5. Variation in effective fringe contrast for four different PSI algorithms as a function of calibration error ε.

Table 1. Summary of Results

Algorithm	ε_{max} (0.01-wave P-V)	ε_{max}' (50% contrast)	N.A.
4	0.04	0.62	0.39
5	0.22	0.58	0.77
7	0.51	0.51	0.95
15	0.88	0.33	0.83

15-bucket algorithms have better than hundredth-wave accuracy with these extreme calibration errors. The 15-bucket algorithm provides phase estimates that are by any practical measure completely insensitive to calibration error; however, it suffers from reduced fringe contrast when $|\varepsilon| > 0.3$.

7. Conclusions

The results of this study are summarized in Table 1. The table includes the maximum calibration error, ε_{max} for hundreth-wave accuracy, an alternative ε_{max}' for a minimum 50% relative fringe contrast, and the maximum N.A. based on the lesser of these two limits. It appears from this table that conventional PSI in a spherical Fizeau cavity is possible with a N.A. of 0.95. This value is considerably larger than that previously supposed in the literature. This purely theoretical conclusion is not meant to trivialize the practical difficulties of working with high-N.A. cavities, which in any case are difficult to align. The analysis does show, however, that the phase-shift calibration problem in spherical cavities is largely solved with modern algorithms.

References

1. J. E. Greivenkamp and J. H. Bruning, "Phase shifting interferometry," in *Optical Shop Testing*, D. Malacara, ed. (Wiley, New York, 1992), Chap. 14, pp. 501–598.
2. R. P. Grosso and R. Crane, "Precise optical evaluation using phase measuring interferometric techniques," in *Interferometry*, G. W. Hopkins, ed., Proc. Soc. Photo-Opt. Instrum. Eng. **192,** 65–74 (1979).
3. P. Hariharan, *Optical Interferometry* (Academic, Orlando, Fla., 1985), Chap. 9, pp. 155–159.
4. K. Kinnstätter, A. W. Lohmann, J. Schwider, and N. Streibl, "Accuracy of phase shifting interferometry," Appl. Opt. **27,** 5082–5089 (1988).
5. C. P. Brophy, "Effect of intensity error correlation on the computed phase of phase-shifting interferometry," J. Opt. Soc. Am. A **7,** 537–541 (1990).
6. L. A. Selberg, "Interferometer accuracy and precision," in *Optical Fabrication and Testing*, D. R. Campbell, C. W. Johnson, and M. Lorenzen, eds., Proc. Soc. Photo-Opt. Instrum. Eng. **1400,** 24–32 (1990).
7. P. de Groot, "Predicting the effects of vibration in phase shifting interferometry," in *Optical Fabrication and Testing Workshop*, Vol. 13 of 1994 OSA Technical Digest Series (Optical Society of America, Washington, D.C., 1994), pp. 189–192.
8. C. L. Koliopoulos, "Avoiding phase-measuring interferometry's pitfalls," Photon. Spectra **22,** 169–176 (1988).
9. Y. Y. Cheng and J. C. Wyant, "Phase shifter calibration in phase-shifting interferometry," Appl. Opt. **24,** 3049–3052 (1985).

10. R. C. Moore and F. H. Slaymaker, "Direct measurement of phase in a spherical-wave Fizeau interferometer," Appl. Opt. **19,** 2196–2200 (1980).
11. K. Creath and P. Hariharan, "Phase-shifting errors in interferometric tests with high-numerical-aperture reference surfaces," Appl. Opt. **33,** 24–25 (1994).
12. P. de Groot, R. Smythe, and L. Deck, "Laser diodes map surface features of complex parts," Laser Focus World, February 1994, pages 95–98.
13. J. Schwider, R. Burow, K.-E. Elssner, J. Grzanna, R. Spolaczyk, and K. Merkel, "Digital wave-front measuring interferometry: some systematic error sources," Appl. Opt. **22,** 3421–3432 (1983).
14. P. Hariharan, B. F. Oreb, and T. Eiju, "Digital phase-shifting interferometry: a simple error-compensating phase calculation algorithm," Appl. Opt. **26,** 2504–2506 (1987).
15. G. Schulz and K.-E. Elssner, "Errors in phase-measurement interferometry with high numerical apertures," Appl. Opt. **30,** 4500–4506 (1991).
16. K. Creath, "Comparison of phase-measurement algorithms," in *Surface Characterization and Testing*, K. Creath, ed., Proc. Soc. Photo-Opt. Instrum. Eng. **680,** 19–28 (1986).
17. K. Creath, "Phase-measurement interferometry techniques," in *Progress in Optics*, E. Wolf, ed. (Elsevier, New York, 1988), Vol. XXVI, Chap. 5, pp. 349–393.
18. J. Schmit and K. Creath, "Some new error-compensating algorithms for phase-shifting interferometry," in *Optical Fabrication and Testing Workshop*, Vol. 13 of 1994 OSA Technical Digest Series (Optical Society of America, Washington, D.C., 1994), paper PD-4.
19. J. van Wingerden, H. H. Frankena, and C. Smorenburg, "Linear approximation for measurement errors in phase shifting interferometry," Appl. Opt. **30,** 2718–2729 (1991).
20. J. Schwider, "Phase shifting interferometry: reference phase error reduction," Appl. Opt. **28,** 3889–3892 (1989).
21. P. de Groot, "Three-color laser-diode interferometer," Appl. Opt. **30,** 3612–3616 (1991).
22. C. Joenathan, "Phase-measuring interferometry: new methods and error analysis," Appl. Opt. **33,** 4147–4155 (1994).
23. J. H. Bruning, D. R. Herriott, J. E. Galllagher, D. P. Rosenfeld, A. D. White, and D. J. Brangaccio, "Digital wavefront measuring interferometer for testing optical surfaces and lenses," Appl. Opt. **13,** 2693–2703 (1974).
24. K. Freischlad and C. L. Koliopoulos, "Fourier description of digital phase-measuring interferometry," J. Opt. Soc. Am. A **7,** 542–551 (1990).
25. J. Schwider, O. Falkenstörfer, H. Schreiber, A. Zöller, and N. Streibl, "New compensating four-phase algorithm for phase-shift interferometry," Opt. Eng. **32,** 1883–1885 (1993).
26. P. de Groot, "Derivation of algorithms for phase-shifting interferometry using the concept of a data sampling window," Appl. Opt. **34** (to be published).
27. P. de Groot and L. Deck, "Long-wavelength laser diode interferometer for surface flatness measurement," in *Optical Measurements and Sensors for the Process Industries*, C. Gorecki and R. W. Preater, eds., Proc. Soc. Photo-Opt. Instrum. Eng. **2248** (1994).
28. C. S. Williams, *Designing Digital Filters* (Prentice-Hall, Englewood Cliffs, N.J., 1986), Chap. 4, p. 113.
29. F. J. Harris, "On the use of windows for harmonic analysis with the discrete Fourier transform," Proc. IEEE **66,** 51–83 (1978).